

Decrease of the organic deuteration during the evolution of Sun-like protostars: the case of SVS13-A

E. Bianchi^{1,2*}, C. Codella¹, C. Ceccarelli^{3,4,1}, F. Fontani¹, L. Testi^{5,1}, R. Bachiller⁶,
B. Lefloch^{3,4}, L. Podio¹, V. Taquet⁷

¹ INAF-Osservatorio Astrofisico di Arcetri, L.go E. Fermi 5, Firenze, 50125, Italy

² Dipartimento di Fisica e Astronomia, Università degli Studi di Firenze, Italy

³ Univ. Grenoble Alpes, IPAG, F-38000 Grenoble, France

⁴ CNRS, IPAG, F-38000 Grenoble, France

⁵ ESO, Karl Schwarzschild str. 2, D-85748 Garching bei Muenchen, Germany

⁶ IGN, Observatorio Astronómico Nacional, Calle Alfonso XIII, 28004 Madrid, Spain

⁷ Leiden Observatory, Leiden University, PO Box 9513, 2300-RA, Leiden, The Netherlands

Accepted date. Received date; in original form date

ABSTRACT

We present the results of formaldehyde and methanol deuteration measurements towards the Class I low-mass protostar SVS13-A, in the framework of the IRAM 30-m ASAI (Astrochemical Surveys At IRAM) project. We detected emission lines of formaldehyde, methanol, and their deuterated forms (HDCO, D₂CO, CHD₂OH, CH₃OD) with E_{up} up to 276 K. The formaldehyde analysis indicates $T_{\text{kin}} \sim 15 - 30$ K, $n_{\text{H}_2} \geq 10^6 \text{ cm}^{-3}$, and a size of about 1200 AU suggesting an origin in the protostellar envelope. For methanol we find two components: (i) a high temperature ($T_{\text{kin}} \sim 80$ K) and very dense ($> 10^8 \text{ cm}^{-3}$) gas from a hot corino (radius $\simeq 35$ AU), and (ii) a colder ($T_{\text{kin}} \leq 70$ K) and more extended (radius $\simeq 350$ AU) region.

The deuterium fractionation is 9×10^{-2} for HDCO, 4×10^{-3} for D₂CO, and $2 - 7 \times 10^{-3}$ for CH₂DOH, up to two orders of magnitude lower than the values measured in Class 0 sources. We derive also formaldehyde deuteration in the outflow: 4×10^{-3} , in agreement with what found in the L1157-B1 protostellar shock. Finally, we estimate $[\text{CH}_2\text{DOH}]/[\text{CH}_3\text{OD}] \simeq 2$. The decrease of deuteration in the Class I source SVS13-A with respect to Class 0 sources can be explained by gas-phase processes. Alternatively, a lower deuteration could be the effect of a gradual collapse of less deuterated external shells of the protostellar envelope. The present measurements fill in the gap between prestellar cores and protoplanetary disks in the context of organics deuteration measurements.

Key words: Molecular data – Stars: formation – radio lines: ISM – submillimetre: ISM – ISM: molecules

1 INTRODUCTION

Deuterium fractionation is the process that enriches the amount of deuterium with respect to hydrogen in molecules. While the D/H elementary abundance ratio is $\sim 1.6 \times 10^{-5}$ (Linsky 2007), for molecules this ratio can be definitely higher and can be a precious tool to understand the chemical evolution of interstellar gas (see e.g. Ceccarelli et al. 2014, and references therein). In particular, during the process leading to the formation of a Sun-like star, large deuteration of formaldehyde and methanol is observed in cold and dense prestellar cores (e.g. Bacmann et al. 2003, Caselli & Ceccarelli 2012, and references therein). Formaldehyde can be formed

through gas phase chemistry in prestellar cores (Roberts & Millar 2000b). The picture is different for formaldehyde as well as for methanol around protostars which are mostly formed via active grain surface chemistry (e.g. Tielens 1983). Deuterated H₂CO and CH₃OH are then stored in the grain mantles to be eventually released into the gas phase once the protostar is formed and the grain mantles are heated and successively evaporated (e.g. Ceccarelli et al. 1998, 2007; Parise et al. 2002, 2004, 2006) or sputtered by protostellar shocks (Codella et al. 2012; Fontani et al. 2014). As a consequence, D/H can be used as fossil record of the physical conditions at the moment of the icy water and organics formation (e.g. Taquet et al. 2012, 2013, 2014).

While deuterated molecules have been detected towards the early stages of the Sun-like star formation (i.e. prestellar cores and

* E-mail: ebianchi@arcetri.astro.it

Class 0 objects) as well as in the Solar System (see e.g. Ceccarelli et al. 2014, and references therein), no clear detection has been obtained for intermediate evolutionary phases (Class I and II objects). A handful of measurements of deuterium fractionation in Class I sources exists (i.e. Roberts & Millar 2007) but they refer only to few transitions sampling large regions (up to $58''$) well beyond the protostellar system. In addition, Loinard et al. (2002) reported measurements of double deuterated formaldehyde in star-forming regions with both the SEST (Swedish ESO Submillimeter telescope) and IRAM single dishes suggesting a decrease with the evolutionary stage. Watanabe et al. (2012) reported the deuterium fractionation measurements toward R CrA IRS7B, a low-mass protostar in the Class 0/I transitional stage. They detected H_2CO , measuring a lower D/H (~ 0.05) compared to deuteration measured in Class 0 objects. However, in this case the low deuterium fractionation ratios do not directly suggest an evolutionary trend. The altered chemical composition of the envelope of R CrA IRS7B can be a result of the heating of the protostar parent core by the external UV radiation from the nearby Herbig Ae star R CrA.

Systematic observations of D/H in Class I objects are therefore required to understand how the deuterium fractionation evolves from prestellar cores to protoplanetary disks. In this context we present a study of formaldehyde and methanol deuteration towards the Class I low-mass protostar SVS13-A.

1.1 The SVS13 star forming region

The SVS13 star forming region is located in the NGC1333 cloud in Perseus at a distance of 235 pc (Hirota et al. 2008). It is associated with a Young Stellar Objects (YSOs) cluster, dominated, in the millimeter by two objects, labelled A, and B, respectively, separated by $\sim 15''$. (see e.g. Chini et al. 1997; Bachiller et al. 1998; Looney et al. 2000; Chen et al. 2009; Tobin et al. 2016, and references therein). Interestingly, SVS13-A and SVS13-B are associated with two different evolutionary stages. On the one hand, SVS13-B is a Class 0 protostar with $L_{\text{bol}} \simeq 1.0 L_{\text{sun}}$ (e.g. Tobin et al. 2016) driving a well collimated SiO jet (Bachiller et al. 1998). On the other hand, SVS13-A is definitely more luminous ($\simeq 32.5 L_{\text{sun}}$, Tobin et al. 2016) and is associated with an extended outflow (> 0.07 pc, Lefloch et al. 1998, Codella et al. 1999) as well as with the well-known chain of Herbig-Haro (HH) objects 7-11 (Reipurth et al. 1993). In addition, SVS13-A has a low $L_{\text{submm}}/L_{\text{bol}}$ ratio ($\sim 0.8\%$) and a high bolometric temperature ($T_{\text{bol}} \sim 188$ K, Tobin et al. 2016). Thus, although still deeply embedded in a large scale envelope (Lefloch et al. 1998), SVS13-A is considered a more evolved protostar, already entered in the Class I stage. For all these reasons, SVS13-A is an almost unique laboratory to investigate how deuteration change from the Class 0 to the Class I phases. In Sect. 2 the IRAM 30-m observations are described, in Sect. 3 we report the results, while in Sect. 4 we develop the analysis of the data; Sect. 5 is for the conclusions.

2 OBSERVATIONS

The observations of SVS13-A were carried out with IRAM 30-m telescope near Pico Veleta (Spain), in the framework of the Astrochemical Surveys At IRAM¹ (ASAI) Large Program. The data consist of an unbiased spectral survey acquired during several runs

between 2012 and 2014, using the broad-band EMIR receivers. In particular the observed bands are at 3 mm (80–116 GHz), 2 mm (129–173 GHz), and 1.3 mm (200–276 GHz). The observations were acquired in wobbler switching mode, with a throw of $180''$ towards the coordinates of SVS13-A, namely $\alpha_{\text{J2000}} = 03^{\text{h}} 29^{\text{m}} 10^{\text{s}}.42$, $\delta_{\text{J2000}} = +31^{\circ} 16' 0''.3$ The pointing was checked by observing nearby planets or continuum sources and was found to be accurate to within $2''$ – $3''$. The telescope HPBWs range between $\simeq 9''$ at 276 GHz to $\simeq 30''$ at 80 GHz. The data reduction was performed using the GILDAS–CLASS² package. Calibration uncertainties are estimated to be $\simeq 10\%$ at 3 mm and $\sim 20\%$ at lower wavelengths. Note that some lines (see Sect. 3) observed at 2 mm and 3 mm (i.e. with a HPBW $\geq 20''$) are affected by emission at OFF position observed in wobbler mode. Line intensities have been converted from antenna temperature to main beam temperature (T_{MB}), using the main beam efficiencies reported in the IRAM 30-m website³.

3 RESULTS

3.1 Line identification

Line identification has been performed using a package developed at IPAG which allows to identify lines in the collected ASAI spectral survey using the Jet Propulsor Laboratory (JPL⁴, Pickett et al. 1998) and Cologne Database for Molecular Spectroscopy (CDMS⁵; Müller et al. 2001, 2005) molecular databases. We double checked the line identifications with the GILDAS Weeds package (Maret et al. 2011). We detected several lines of H_2^{13}CO , HDCO, D_2CO , $^{13}\text{CH}_3\text{OH}$ and CH_2DOH (see Tables 1 and 2). Examples of the detected line profiles in T_{MB} scale are shown in Figure 1. The peak velocities of the detected lines are between $+8$ km s^{-1} and $+9$ km s^{-1} , being consistent, once considered the fit uncertainties, with the systemic velocity of both A and B component of SVS13 ($+8.6$ km s^{-1} , Chen et al. 2009; López-Sepulcre et al. 2015). We fitted the lines with a Gaussian function, and excluded from the analysis those lines with $|v_{\text{peak}} - v_{\text{sys}}| > 0.6$ km/s plausibly affected by line blending. We select for the analysis only the lines with a signal to noise (S/N) higher than 4σ . The spectral parameters of the detected lines, as well as the results from the Gaussian fits, are presented in Tables 1 and 2, where we report the frequency of each transition (GHz), the telescope HPBW ($''$), the excitation energies of the upper level E_{up} (K), the $S\mu^2$ product (D^2), the line rms (mK), the peak temperature (mK), the peak velocities (km s^{-1}), the line full width at half maximum (FWHM) (km s^{-1}) and the velocity integrated line intensity I_{int} (mK km s^{-1}).

3.2 Formaldehyde isotopologues

We report the detection of several lines of H_2CO and its isotopologues H_2^{13}CO , HDCO and D_2CO . The measured intensity ratio between the low energy transitions of H_2CO and H_2^{13}CO (as e.g. the $3_{1,3}-2_{1,2}$ at $E_{\text{up}} = 32$ K), is ~ 25 , a value well below the median value for the interstellar medium of $^{12}\text{C}/^{13}\text{C} \sim 68$ (Milam et al. 2005). This indicates that the observed H_2CO transitions are optically thick. Therefore we use H_2^{13}CO to derive the formaldehyde deuteration.

² <http://www.iram.fr/IRAMFR/GILDAS>

³ <http://www.iram.es/IRAMES/mainWiki/Iram30mEfficiencies>

⁴ <https://spec.jpl.nasa.gov/>

⁵ <http://www.astro.uni-koeln.de/cdms/>

¹ www.oan.es/asai

We detected 7 lines of H_2^{13}CO , 5 lines of HDCO and 5 lines of D_2CO , with excitation energies, E_{up} , in the 10–45 K range. Examples of the detected line profiles are shown in Figure 1; the detected transitions and the observational parameters are displayed in Table 1 and Table 2. The lines profiles are close to a gaussian shape and the peak velocities are close to the systemic source velocity with values between $+7.8 \text{ km s}^{-1}$ and $+9.0 \text{ km s}^{-1}$ while the FWHM is between 0.9 and 2.5 km s^{-1} . Three lines of H_2^{13}CO (with frequencies 137.45 GHz, 141.98 GHz, and 146.64 GHz) and one line of HDCO (with frequency 134.2848) are detected in the 2 mm band and they are affected by contamination of emission in the off positions (see Sect. 2 for details on the observing techniques), consistently with the analysis reported by López-Sepulcre et al. (2015), using ASAI spectra. The contaminated lines correspond to a size of the telescope HPBW $> 16''$. In these cases the measured intensities will be treated as lower limits in the rotational diagram analysis (see Sect. 4.2). For the D_2CO , only one line is detected at 2 mm but it does not show any absorption feature due to the wobbler contamination. This can be an indication of a more compact region emitting in D_2CO with respect to that of HDCO emission. A similar behaviour has been observed in a different context by Fuente et al. (2015) towards the intermediate-mass Class 0 protostar NGC 7129FIRS 2. They detected, using interferometric observations, an intense and compact D_2CO component associated with the hot core. On the other hand Ceccarelli et al. (2001) detected in the low-mass Class 0 protostar IRAS16293-2422, an extended D_2CO emission (up to $\sim 5000 \text{ AU}$), associated with the external envelope. The present data do not allow us to draw reliable conclusions on the relative size of the two deuterated formaldehyde isotopologues. However, in the case of SVS13-A a more compact size is suggested by the broader line profiles of D_2CO with respect to HDCO (see Figure 2). In Figure 2 we show the distribution of the linewidths of the detected HDCO lines in hatched blue and D_2CO lines in cyano. The bulk of the HDCO lines has a FWHM between 1.5 and 2.0 km s^{-1} while for the D_2CO the peak of the distribution is in the $2.0\text{--}2.5 \text{ km s}^{-1}$ range. A further discussion on this will be done in Section 4 following the results of the rotational diagram analysis.

Interestingly, three lines of low excitation ($E_{\text{up}} < 35 \text{ K}$) of H_2^{13}CO (with frequencies 212.81 GHz, 206.13 GHz and 219.91 GHz) and all the HDCO lines (except for the line in the 2 mm band) show weak ($\sim 30 \text{ mK}$) wings clearly indicating emission due to outflows that we analyse separately from the main line component.

3.3 Methanol isotopologues

Similarly to formaldehyde, the detected lines of CH_3OH are optically thick. We verified it through the measured ratio between the intensities of CH_3OH and $^{13}\text{CH}_3\text{OH}$ (as e.g. the $5_{1,5}\text{--}4_{1,4} + +$ at $E_{\text{up}} = 49 \text{ K}$) that is ~ 2 . For this reason also in this case, we use $^{13}\text{CH}_3\text{OH}$ to calculate methanol column density. In the case of methanol, the process of line identification was more complex than formaldehyde. This is due to the very rich spectra observed with ASAI towards SVS13-A with a consequent challenging lines identification for a complex molecule such as CH_3OH . In addition to the criteria summarized in Section 3.1, we further require $\text{FWHM} > 2 \text{ km s}^{-1}$ to discard any possible false identification. For transitions with multiple components (e.g. $^{13}\text{CH}_3\text{OH } 2_{1,1}\text{--}1_{1,0}$ and $2_{1,1}\text{--}1_{1,0}\text{--}$) we select only the lines for which the different component intensities are close to the expected LTE (Local Thermodynamic Equilibrium) relative intensities.

We report the detection of 18 transitions of $^{13}\text{CH}_3\text{OH}$ and 27

lines of CH_2DOH with excitation energies in the 20–276 K range. Examples of the detected line profiles for methanol isotopologues are shown in Figure 1. The spectral parameters and the results of the gaussian fit are shown in Tables 1 and 2. The line profiles are broader than for formaldehyde isotopologues, with a FWHM up to 5.4 km s^{-1} . None of the observed profiles show absorption features due to the wobbler contamination, pointing to an emitting region smaller than formaldehyde.

Interestingly, we detect two different transitions of both CHD_2OH and CH_3OD with E_{up} between 33 K and 77 K (see Table 1 and Figure 3). The peak velocities are consistent with the systemic source velocity and the FWHMs are in agreement with those of the lines from the other methanol isotopologues.

3.4 Summary of the results

In summary, the bulk of methanol and formaldehyde isotopologues lines are detected in the 1 mm band. For this reason, the temperature estimate from the rotational diagram analysis (see Section 4.2) is not affected by the beam dilution. The 30-m HPBW is $\sim 10''$ at 1 mm, which ensures that the emission is coming from SVS13-A with no contamination from SVS13-B (the separation between SVS13-A and the companion protostar is $\sim 15''$). The lines collected in the 2 and 3 mm bands could be contaminated by the emission from SVS13-B, because the HPBW is larger, but they are only a handful of lines.

Interestingly, the formaldehyde profiles show line wings that suggest emission due to the extended outflow driven by SVS13-A ($> 0.07 \text{ pc}$, Lefloch et al. 1998, Codella et al. 1999).

4 DISCUSSION

4.1 LVG analysis

We analysed the H_2^{13}CO and $^{13}\text{CH}_3\text{OH}$ observed lines with the non-LTE Large Velocity Gradient (LVG) approach using the model described in Ceccarelli et al. (2003). For methanol we used the $\text{CH}_3\text{OH}\text{--H}_2$ collisional coefficients provided by the BASECOL database (Dubernet et al. 2013). In the case of formaldehyde, we considered only the ortho form, for which the $\text{H}_2\text{CO}\text{--H}_2$ collisional coefficients (Troscompt et al. 2009a) are available. We assumed a Boltzmann distribution for the H_2 , using for the methanol analysis the statistical ortho-to-para ratio of 3. In the case of formaldehyde we assumed a ortho-to-para ratio close to zero following Troscompt et al. (2009b). We ran grids of models varying the kinetic temperature, T_{kin} , (from 10 to 200 K), the H_2 density, n_{H_2} , (from 10^4 to 10^{10} cm^{-3}), the H_2^{13}CO column density, $N(^{13}\text{H}_2\text{CO})$, (from 10^{11} to 10^{13} cm^{-2}), and the $^{13}\text{CH}_3\text{OH}$ column density, $N(^{13}\text{CH}_3\text{OH})$, (from 10^{16} to 10^{18} cm^{-2}), while the emitting size, θ_s , was left as free parameter.

In the case of formaldehyde, the best fit was obtained with $N(^{13}\text{H}_2\text{CO}) = 5.5 \times 10^{12} \text{ cm}^{-2}$ and $\theta_s = 5'' \pm 1''$. Figure 4 (upper panel) shows the χ_r^2 contour plot as a function of the temperature and H_2 density using these values. The temperatures corresponding to the best fit solution are $T_{\text{kin}} = 20\text{--}25 \text{ K}$ and the density are quite high $n_{\text{H}_2} \simeq 0.2\text{--}2 \times 10^7 \text{ cm}^{-3}$, suggesting to be close to LTE. Figure 4 (lower panel) shows, for the best fit solution, the ratio between the measured lines intensities and the LVG model predictions, as a function of the line upper level energy. The detected transitions are predicted to be optically thin (opacities between 0.03 and 0.06).

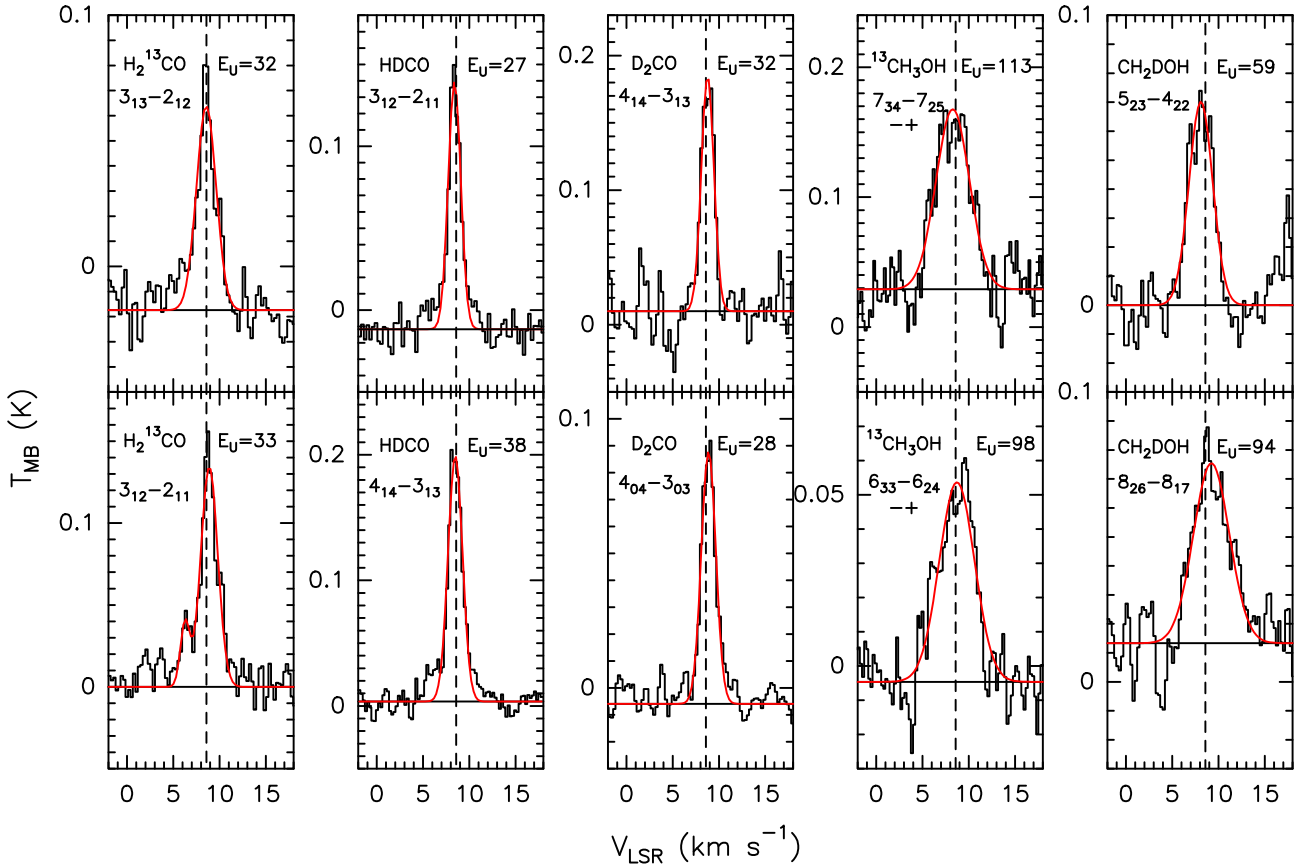


Figure 1. Examples of line profiles in T_{MB} scale (not corrected for the beam dilution): species and transitions are reported. The vertical dashed line stands for the ambient LSR velocity ($+8.6 \text{ km s}^{-1}$, Chen et al. 2009)

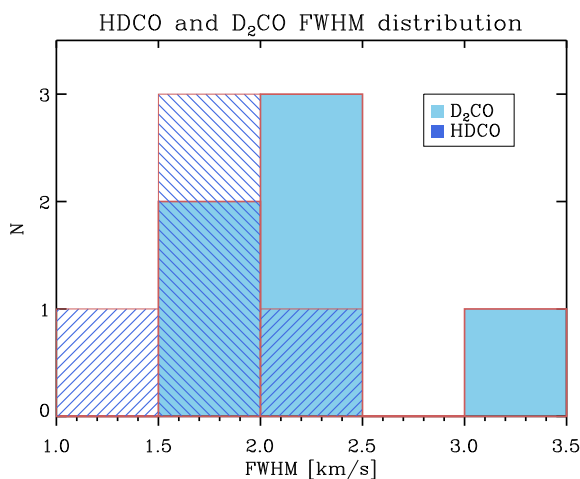


Figure 2. Distribution of the linewidth (FWHM) of the observed HDCO and D_2CO lines. Cyan is for D_2CO and blue hatched is for HDCO.

The LVG analysis clearly supports the association of formaldehyde with the protostellar envelope with a size of $\sim 1200 \text{ AU}$.

Different is the case of $^{13}\text{CH}_3\text{OH}$ for which the LVG model does not converge towards a solution suggesting we are mixing emission from different regions, possibly due to different HPBW.

Following this suggestion, we considered separately the lines with higher excitations ($E_{\text{up}} > 40 \text{ K}$) observed with similar HPBWs (between $9''$ and $15''$). The solution with the lowest χ_r^2 corresponds to $N(^{13}\text{CH}_3\text{OH}) = 9 \times 10^{16} \text{ cm}^{-2}$ and an emitting size of $\theta_s = 0''.3 \pm 0''.1$, i.e. a radius of 35 AU (see Figure 5). The best fit solution corresponds to a temperature of $T_{\text{kin}} = 80 \text{ K}$ and very high-densities, $n_{\text{H}_2} \geq 10^8 \text{ cm}^{-3}$. The line opacities vary from 0.8 to 2.5, being thus moderately optically thin. All these values suggest that the emission detected at high excitations is dominated by a hot corino, an environment which is typically very abundant in methanol, due to thermal evaporation of the dust mantles (e.g. Caselli & Ceccarelli 2012). Interestingly, the occurrence of a hot-corino around SVS13-A has been recently suggested by high-excitation HDO lines, also observed in the ASAI context and indicating a T_{kin} larger than 150 K on smaller spatial scales (a radius $\sim 25 \text{ AU}$; Codella et al. 2016).

The analysis of the remaining 4 lines (observed with HPBWs larger than $15''$) is not straightforward given the 4 transitions have almost the same E_{up} ($20 - 28 \text{ K}$). The LVG approach suggests typical solutions with column densities of $N(^{13}\text{CH}_3\text{OH}) \sim 10^{15} \text{ cm}^{-2}$, temperatures $\leq 70 \text{ K}$, densities at least 10^6 cm^{-3} , and sizes $\simeq 2'' - 4''$. The line opacities in this case range from 0.007 to 0.02, being thus optically thin. The lower densities and the more extended emitting size suggest that we are sampling a more extended region (a radius $\sim 350 \text{ AU}$) around the protostar where the temperature is still high enough to allow the methanol molecules to be released from grain mantles.

Table 1. List of transitions and line properties (in T_{MB} scale) of the HDCO, D₂CO and CH₂DOH emission detected towards SVS13-A

Transition	ν^a (GHz)	HPBW ($''$)	E_{up}^a (K)	$S\mu^{2a}$ (D ²)	rms (mK)	T_{peak}^b (mK)	V_{peak}^b (km s ⁻¹)	$FWHM^b$ (km s ⁻¹)	I_{int}^b (mK km s ⁻¹)
Deuterated species									
HDCO 2 _{1,1} -1 _{1,0}	134.2848	18	18	8	17	158(5)	+8.31(0.05)	1.1(0.1)	188(17)
HDCO 3 _{1,2} -2 _{1,1}	201.3414	12	27	14	19	334(22)	+8.43(0.03)	1.6(0.1)	561(21)
HDCO 4 _{1,4} -3 _{1,3}	246.9246	10	38	20	17	312(22)	+8.50(0.03)	1.9(0.1)	619(18)
HDCO 4 _{0,4} -3 _{0,3}	256.5854	10	31	22	10	376(20)	+8.54(0.01)	1.9(0.0)	777(11)
HDCO 4 _{1,3} -3 _{1,2}	268.2920	9	40	20	21	207(21)	+8.55(0.05)	2.0(0.1)	451(23)
p-D ₂ CO 3 _{1,3} -2 _{1,2}	166.1028	15	21	14	11	33(9)	+8.79(0.21)	2.2(0.5)	79(15)
p-D ₂ CO 4 _{1,4} -3 _{1,3}	221.1918	11	32	20	16	92(7)	+8.74(0.09)	1.8(0.2)	178(17)
o-D ₂ CO 4 _{0,4} -3 _{0,3}	231.4103	11	28	43	11	194(12)	+8.88(0.03)	1.9(0.1)	381(12)
o-D ₂ CO 4 _{2,2} -3 _{2,1}	236.1024	10	50	33	13	56(7)	+8.95(0.13)	2.4(0.3)	144(16)
p-D ₂ CO 4 _{1,3} -3 _{1,2}	245.5329	10	35	20	11	55(7)	+8.85(0.11)	2.4(0.3)	139(13)
CH ₂ DOH 2 _{0,2} -1 _{0,1} e1	89.2753	28	20	1	3	12(2)	+8.65(0.37)	4.2(1.1)	51(9)
CH ₂ DOH 6 _{1,5} -6 _{0,6} e0	99.6721	25	50	7	2	15(2)	+8.09(0.17)	4.1(0.5)	68(6)
CH ₂ DOH 7 _{1,6} -7 _{0,7} e0	105.0370	23	65	8	3	17(3)	+8.66(0.18)	3.1(0.4)	57(6)
CH ₂ DOH 3 _{1,2} -2 _{1,1} e1	135.4529	18	29	2	8	30(6)	+8.48(0.22)	3.0(0.5)	98(15)
CH ₂ DOH 3 _{1,3} -4 _{0,4} e1	161.6025	15	29	1	9	36(7)	+8.71(0.19)	2.7(0.4)	103(15)
CH ₂ DOH 5 _{1,5} -4 _{1,4} o1	221.2730	11	55	4	17	57(7)	+8.31(0.19)	3.2(0.4)	195(22)
CH ₂ DOH 5 _{0,5} -4 _{0,4} e1	222.7415	11	46	4	10	75(8)	+8.45(0.10)	4.3(0.2)	342(15)
CH ₂ DOH 5 _{2,3} -4 _{1,4} e0	223.0711	11	48	3	8	59(9)	+7.98(0.11)	4.5(0.2)	284(13)
CH ₂ DOH 5 _{3,3} -4 _{3,2} o1 ^c	223.1535	11	87	2	10	56(7)	+8.34(0.13)	3.8(0.3)	223(15)
CH ₂ DOH 5 _{3,2} -4 _{3,1} o1 ^c	223.1536	11	87	2	10	56(7)	+8.34(0.13)	3.8(0.3)	223(15)
CH ₂ DOH 5 _{2,3} -4 _{2,2} e1	223.3155	11	59	3	12	70(8)	+8.12(0.10)	3.0(0.2)	228(15)
CH ₂ DOH 5 _{4,2} -4 _{1,1} e0 ^c	223.6162	11	95	1	10	47(11)	+8.25(0.14)	3.5(0.3)	174(14)
CH ₂ DOH 5 _{4,1} -4 _{0,0} e0 ^c	223.6162	11	95	1	10	47(11)	+8.25(0.14)	3.5(0.3)	174(14)
CH ₂ DOH 5 _{1,4} -4 _{1,3} e1	225.6677	11	49	4	11	56(11)	+8.18(0.15)	4.0(0.3)	237(17)
CH ₂ DOH 5 _{1,4} -4 _{1,3} e0	226.8183	11	37	3	10	51(10)	+8.08(0.14)	3.8(0.3)	203(14)
CH ₂ DOH 15 _{2,13} -15 _{1,14} e0	228.2461	11	276	20	29	89(12)	+7.84(0.20)	3.0(0.4)	285(37)
CH ₂ DOH 9 _{2,7} -9 _{1,8} e0	231.9692	11	113	11	14	99(8)	+8.72(0.09)	3.7(0.2)	390(19)
CH ₂ DOH 8 _{2,6} -8 _{1,7} e0	234.4710	10	94	10	13	67(8)	+9.17(0.14)	4.1(0.3)	293(19)
CH ₂ DOH 7 _{2,5} -7 _{1,6} e0	237.2499	10	76	8	12	64(12)	+8.31(0.13)	3.9(0.3)	266(18)
CH ₂ DOH 7 _{1,6} -6 _{2,4} o1	244.5884	10	83	2	16	61(10)	+8.09(0.18)	3.6(0.6)	231(26)
CH ₂ DOH 3 _{2,1} -3 _{1,2} e0	247.6258	10	29	2	9	48(8)	+8.26(0.13)	3.7(0.3)	189(13)
CH ₂ DOH 3 _{2,2} -3 _{1,3} e0	255.6478	10	29	2	9	58(8)	+8.61(0.12)	5.3(0.4)	331(16)
CH ₂ DOH 4 _{1,4} -3 _{0,3} e0	256.7316	10	25	3	9	61(8)	+8.32(0.11)	4.3(0.2)	278(14)
CH ₂ DOH 4 _{2,3} -4 _{1,4} e0	258.3371	10	38	3	14	60(6)	+8.33(0.16)	4.7(0.4)	302(21)
CH ₂ DOH 5 _{2,4} -5 _{1,5} e0	261.6874	9	48	4	17	45(9)	+8.09(0.26)	4.3(0.5)	205(24)
CH ₂ DOH 13 _{0,13} -12 _{1,12} e0	262.5969	9	194	5	17	54(12)	+8.51(0.21)	3.8(0.4)	219(23)
CH ₂ DOH 6 _{1,6} -5 _{1,5} e0	264.0177	9	48	4	14	64(7)	+8.40(0.12)	2.8(0.3)	192(17)
CH ₂ DOH 7 _{2,6} -7 _{1,7} e0	270.2999	9	76	6	14	55(13)	+8.35(0.17)	4.2(0.4)	243(19)
CH ₂ DOH 6 _{1,5} -5 _{1,4} e1	270.7346	9	62	4	16	60(10)	+8.21(0.16)	3.5(0.3)	222(20)
CHD ₂ OH 5 ₀ -4 ₀ e1	207.771	11	48	4	14	43(9)	+8.69(0.20)	2.7(0.4)	125(17)
CHD ₂ OH 5 ₃ -4 ₃ e1 ^c	207.868	11	77	2	11	35(10)	+7.21(0.24)	4.1(0.5)	153(17)
CHD ₂ OH 5 ₃ -4 ₃ e1 ^c	207.869	11	77	2	11	35(10)	+7.21(0.24)	4.1(0.5)	153(17)
CH ₃ OD 5 ₁₊ -4 ₁₊	223.3086	11	39	3	20	32(10)	+8.53(0.41)	3.2(0.9)	108(27)
CH ₃ OD 5 ₀₊ -4 ₀₊	226.5387	11	33	4	18	48(10)	+8.87(0.28)	4.6(0.6)	232(28)

^a Frequencies and spectroscopic parameters of HDCO and D₂CO have been extracted from the Cologne Database for Molecular Spectroscopy (Müller et al. 2005). Those of CH₂DOH are extracted from the Jet Propulsion Laboratory database (Pickett et al. 1998). ^b The errors in brackets are the gaussian fit uncertainties. ^c The lines cannot be distinguished with the present spectral resolution.

4.2 Rotational Diagram analysis

The LVG analysis previously described suggests LTE conditions and optically thin lines. As a consequence we used the rotational diagram analysis to determine the temperature and the column density of formaldehyde and methanol isotopologues through a more direct approach. For a given molecule, the relative population dis-

tribution of all the energy levels, is described by a Boltzmann temperature, that is the rotational temperature T_{rot} . The upper level column density can be written as:

$$N_u = \frac{8\pi k\nu^2}{hc^3 A_{ul}} \frac{1}{\eta_{bf}} \int T_{mb} dV \quad (1)$$

Table 2. List of transitions and line properties (in T_{MB} scale) of the H_2^{13}CO and $^{13}\text{CH}_3\text{OH}$ emission towards SVS13-A

Transition	ν^a (GHz)	HPBW ($''$)	E_{up}^a (K)	$S\mu^{2a}$ (D^2)	rms (mK)	T_{peak}^b (mK)	V_{peak}^b (km s^{-1})	$FWHM^b$ (km s^{-1})	I_{int}^b (mK km s^{-1})
Isotopologues									
$\text{o-H}_2^{13}\text{CO } 2_{1,2}-1_{1,1}$	137.4500	18	22	24	10	63(4)	+8.50(0.08)	1.0(0.2)	64 (10)
$\text{p-H}_2^{13}\text{CO } 2_{0,2}-1_{0,1}$	141.9837	17	10	11	10	54 (10)	+8.46(0.10)	1.1(0.2)	62(10)
$\text{o-H}_2^{13}\text{CO } 2_{1,1}-1_{1,0}$	146.6357	17	22	24	14	105(4)	+8.39(0.06)	0.9(0.1)	98(13)
$\text{o-H}_2^{13}\text{CO } 3_{1,3}-2_{1,2}$	206.1316	12	32	44	13	124(15)	+8.58(0.06)	2.5(0.2)	332(18)
$\text{p-H}_2^{13}\text{CO } 3_{0,3}-2_{0,2}$	212.8112	12	20	16	10	70(6)	+7.76(0.14)	2.0(0.3)	235(65)
$\text{o-H}_2^{13}\text{CO } 3_{1,2}-2_{1,1}$	219.9085	11	33	43	10	134(12)	+8.90(0.04)	2.2(0.1)	359(17)
$\text{o-H}_2^{13}\text{CO } 4_{1,4}-3_{1,3}$	274.7621	10	45	31	21	102(16)	+8.34(0.11)	2.5(0.3)	270(25)
$^{13}\text{CH}_3\text{OH } 2_{0,2}-1_{0,1}$	94.4110	26	20	2	2	10(2)	+8.61(0.21)	3.9 (0.4)	42(4)
$^{13}\text{CH}_3\text{OH } 2_{1,1}-1_{1,0}$	94.4205	26	28	1	2	11(1)	+9.19(0.16)	2.4(0.4)	27(4)
$^{13}\text{CH}_3\text{OH } 2_{1,1}-1_{1,0}-$	95.2087	26	21	1	2	17(2)	+7.56(0.10)	3.5(0.3)	65(4)
$^{13}\text{CH}_3\text{OH } 1_{1,0}-1_{0,1}$	165.5661	15	23	1	8	76(8)	+8.58(0.09)	3.6(0.2)	289(15)
$^{13}\text{CH}_3\text{OH } 7_{1,6}-7_{0,7}$	166.5695	15	84	6	5	34(5)	+8.64(0.13)	3.5(0.4)	125(10)
$^{13}\text{CH}_3\text{OH } 8_{-1,8}-7_{0,7}$	221.2852	11	87	5	11	49(11)	+8.05(0.16)	3.5(0.3)	180(16)
$^{13}\text{CH}_3\text{OH } 5_{1,5}-4_{1,4}++$	234.0116	11	48	4	10	66(13)	+8.87(0.11)	4.1(0.3)	284(16)
$^{13}\text{CH}_3\text{OH } 5_{0,5}-4_{0,4}$	235.8812	10	47	4	13	70(8)	+9.11(0.12)	3.3(0.3)	245(17)
$^{13}\text{CH}_3\text{OH } 5_{-1,5}-4_{-1,4}$	235.9382	10	40	4	10	52(10)	+8.84(0.15)	5.0(0.3)	275(17)
$^{13}\text{CH}_3\text{OH } 10_{3,7}-10_{2,8}++$	254.5094	10	175	9	8	54(7)	+8.31(0.09)	3.7(0.2)	215(10)
$^{13}\text{CH}_3\text{OH } 8_{3,5}-8_{2,6}++$	254.8418	10	132	7	7	52(7)	+8.29(0.09)	4.0(0.2)	218(11)
$^{13}\text{CH}_3\text{OH } 7_{3,4}-7_{2,5}++$	254.9594	10	113	6	11	52(7)	+8.25(0.14)	4.3(0.3)	238(15)
$^{13}\text{CH}_3\text{OH } 6_{3,3}-6_{2,4}++$	255.0510	10	98	5	10	71(11)	+8.63(0.11)	4.7(0.2)	353(16)
$^{13}\text{CH}_3\text{OH } 8_{3,6}-8_{2,7}++$	255.2656	10	132	7	6	47(6)	+8.30(0.09)	3.9(0.2)	193(9)
$^{13}\text{CH}_3\text{OH } 9_{3,7}-9_{2,8}++$	255.3559	10	152	8	7	51(7)	+8.52(0.09)	3.8(0.2)	208(11)
$^{13}\text{CH}_3\text{OH } 10_{3,8}-10_{2,9}++$	255.4970	10	175	9	9	46(9)	+8.43(0.14)	4.1(0.3)	202(13)
$^{13}\text{CH}_3\text{OH } 5_{2,3}-4_{1,3}$	263.1133	9	56	4	10	60(10)	+8.31(0.12)	4.4(0.3)	278(15)
$^{13}\text{CH}_3\text{OH } 9_{-1,9}-8_{0,8}$	268.6354	9	107	6	13	55(13)	+7.99(0.16)	4.1(0.4)	236(18)

^a Frequencies and spectroscopic parameters of H_2^{13}CO and $^{13}\text{CH}_3\text{OH}$ have been extracted from the Cologne Database for Molecular Spectroscopy (Müller et al. 2005). Upper level energies refer to the corresponding ground state of each symmetry. ^b The errors in brackets are the gaussian fit uncertainties.

where k is the Boltzmann constant, ν is the frequency of the transition, h is the Plank constant, c is the light speed, A_{ul} is the Einstein coefficient, η_{bf} ⁶ is the beam-filling factor and the integral is the integrated line intensities.

N_u is related to the rotational temperature T_{rot} , as follow:

$$\ln \frac{N_u}{g_u} = \ln N_{\text{tot}} - \ln Q(T_{\text{rot}}) - \frac{E_{\text{up}}}{kT_{\text{rot}}} \quad (2)$$

where g_u is the generacy of the upper level, N_{tot} is the total column density of the molecule, $Q(T_{\text{rot}})$ is the partition function at the rotational temperature and E_{up} is the energy of the upper level.

As a first step we assumed a size filling the smaller IRAM 30-m beam, i.e. $10''$, a value consistent with the continuum emission at 1.25 mm observed with IRAM 30-m radiotelescope by Lefloch et al. (1998). Note however that the T_{rot} estimate does not depend on the source size assumption because almost all the lines have been observed with a beam of $\sim 10''$ and then suffer the same beam dilution. The rotational diagram analysis shows low values of T_{rot} , around 20 K, consistent with the LVG results and consistent with an association with the extended molecular envelope around the protostar. We obtained $T_{\text{rot}} = 23 \pm 4$ K and column density $N_{\text{tot}} = 25 \pm 6 \times 10^{11} \text{ cm}^{-2}$ (H_2^{13}CO), $T_{\text{rot}} = 15 \pm 2$ K and $N_{\text{tot}} = 9 \pm 3 \times 10^{12} \text{ cm}^{-2}$ (HD CO), and $T_{\text{rot}} = 28 \pm 6$ K and column density $N_{\text{tot}} = 13 \pm 3 \times 10^{11} \text{ cm}^{-2}$ (D_2CO), see Figure 6.

⁶ $\eta_{bf} = \theta_s^2 \times (\theta_s^2 + \theta_b^2)^{-1}$; θ_s and θ_b are the source and the beam sizes (assumed to be both a circular Gaussian).

For HD CO we detected line wings with velocities up to $\sim \pm 3 \text{ km s}^{-1}$ with respect to the systemic source velocity. This low velocity emission is likely probing ambient material swept-up by the outflow associated with SVS13-A (Lefloch et al. 1998). We derived the temperature and column density of this outflow component using the residual intensities after subtracting the gaussian fit of the ambient component and then we analysed them separately. From the rotational diagram analysis we obtained for both the blue- and the red-shifted emission, a $T_{\text{rot}} \sim 12$ K. Also in this case, the T_{rot} value is not affected by beam dilution because the lines come from the 1.3 mm band. The low T_{rot} value is again an indication of an extended emission, in agreement with the well-studied extended outflow driven by SVS13-A (Lefloch et al. 1998). We assumed also in this case an arbitrary source size of $10''$, obtaining $T_{\text{rot}} = 12 \pm 7$ K and $N_{\text{tot}} = 9 \pm 15 \times 10^{11} \text{ cm}^{-2}$ (HD CO blue wing), $T_{\text{rot}} = 12 \pm 8$ K and $N_{\text{tot}} = 6 \pm 12 \times 10^{11} \text{ cm}^{-2}$ (HD CO red wing). In the case of H_2^{13}CO , due to line contamination, we detected blue wings only for two lines; by assuming the same rotational temperature of the HD CO wings, we obtained a column density of $N_{\text{tot}} \sim 9 \times 10^{10} \text{ cm}^{-2}$.

For H_2^{13}CO and HD CO we detect both para and ortho transitions (see Tables 1 and 2). Once considered both species in a single rotation diagram, the distribution does not show any significant scatter from the linear fit. Considering the poor statistic (2 para and 5 ortho transitions for H_2^{13}CO ; 3 para and 2 ortho transitions for HD CO) and the uncertainties of the line intensities, this is consistent with the o/p statistical values at the high-temperature limit (3:1 for H_2^{13}CO and 2:1 for D_2CO).

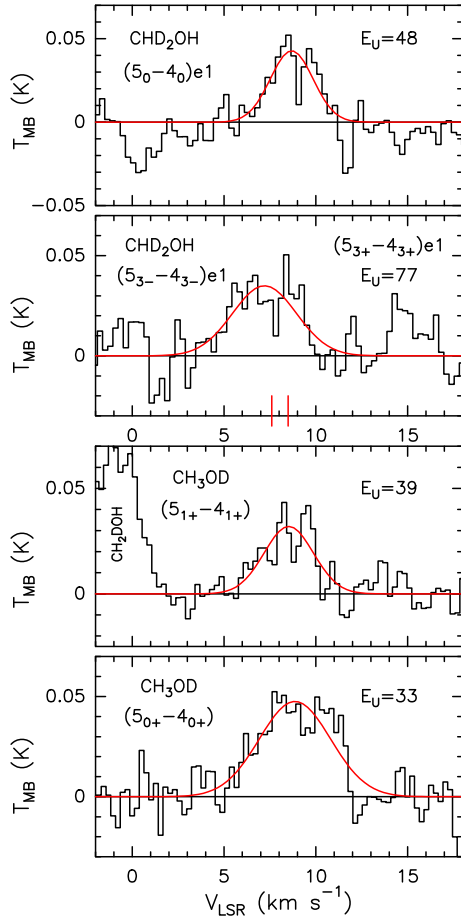


Figure 3. Tentative detections of emission due to CHD₂OH (upper panel) and CH₃OD (lower panel) transitions. Transitions and upper level energies are reported. Red curves are for the Gaussian fit. Note that the middle-upper panel reports emission due to two different transitions (see the red vertical bars).

For the methanol analysis one rotational temperature is not able to fit the rotational diagrams of ¹³CH₃OH and CH₂DOH, supporting the occurrence of two emitting components associated with different excitation conditions, as already suggested by the LVG analysis.

A better fit is obtained using two slopes (see Figure 7; again as a first step assuming a source size of 10''):

(i) one with a low T_{rot} (15 ± 3 K for ¹³CH₃OH and 27 ± 8 K for CH₂DOH) for the lines with $E_{\text{up}} < 50$ K. The column densities are $N_{\text{tot}} = 18 \pm 7 \times 10^{13} \text{ cm}^{-2}$ for ¹³CH₃OH and $N_{\text{tot}} = 11 \pm 5 \times 10^{13} \text{ cm}^{-2}$ for CH₂DOH;

(ii) one with a higher T_{rot} (99 ± 13 K for ¹³CH₃OH and 190 ± 76 K for CH₂DOH) for the lines with $E_{\text{up}} > 50$ K. The column densities are $N_{\text{tot}} = 4 \pm 1 \times 10^{14} \text{ cm}^{-2}$ for ¹³CH₃OH and $N_{\text{tot}} = 8 \pm 2 \times 10^{14} \text{ cm}^{-2}$ for CH₂DOH.

These two excitation regimes are in agreement with what found with the LVG approach: a hot corino and a more extended region associated with a lower temperature. The higher T_{rot} values obtained for both ¹³CH₃OH and CH₂DOH with respect to the formaldehyde isotopologues suggest again that the origin of the emission is not the extended envelope but the hot corino.

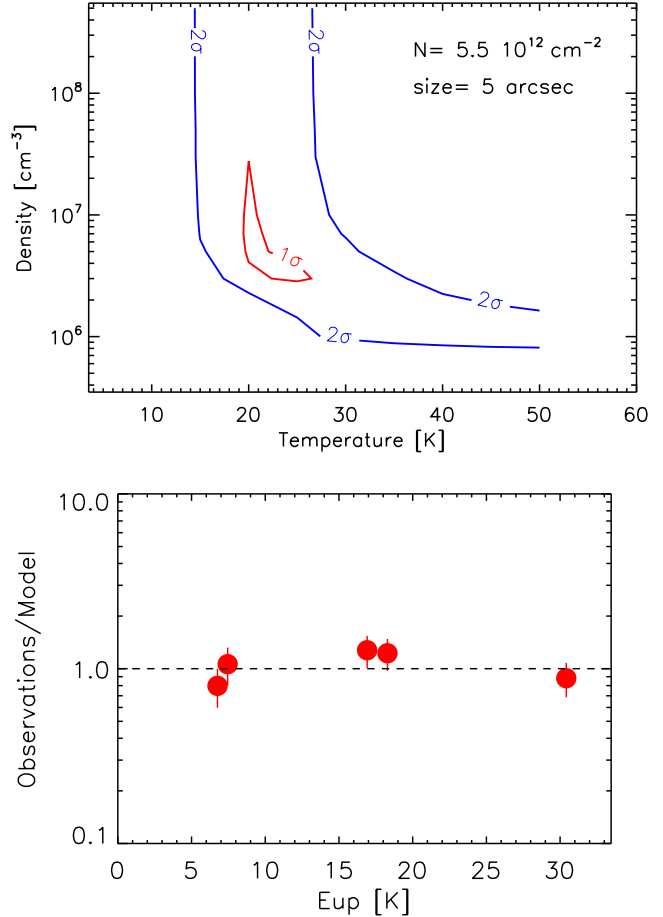


Figure 4. *Upper panel:* The 1σ and 2σ contour plot of χ^2 obtained considering the non-LTE model predicted and observed intensities of all the detected ortho ¹³H₂CO lines. The best fit is obtained with $N(^{13}\text{H}_2\text{CO}) = 5.5 \times 10^{12} \text{ cm}^{-2}$, $\theta_s = 5''$, $T_{\text{kin}} = 20$ K and $n_{\text{H}_2} \geq 7 \times 10^6 \text{ cm}^{-3}$. *Lower panel:* Ratio between the observed line intensities with those predicted by the best fit model as a function of line upper level energy E_{up} .

4.3 Methanol and formaldehyde deuteration

We use the column densities derived from the rotation diagrams to derive the D/H ratio for formaldehyde and methanol. In order to properly measure the D/H, the column densities are derived assuming for each species, the source size suggested by the LVG analysis: 5'' for formaldehyde isotopologues, $\sim 3''$ for methanol lines with $E_{\text{up}} < 50$ K and 0'.3 for methanol lines with $E_{\text{up}} > 50$ K. As already discuss in Section 3, it was not possible to directly measure the column density of the main isotopologue of H₂CO and CH₃OH because the lines are optically thick. For this reason we derived the formaldehyde and methanol column densities from the H₂¹³CO and ¹³CH₃OH column densities, assuming a ¹²C/¹³C ratio of 86 (Milam et al. 2005) at the galactocentric distance of SVS13-A.

We report the obtained D/H ratios in Table 3. To be consistent, we assumed for the D-species the T_{rot} derived from the ¹³C-isotopologues. In any case the following conclusions do not change if we assume for all the molecules the corresponding T_{rot} .

For H₂CO we measured a D/H of $9 \pm 4 \times 10^{-2}$. We can compare this value with measurements of deuterated formaldehyde in

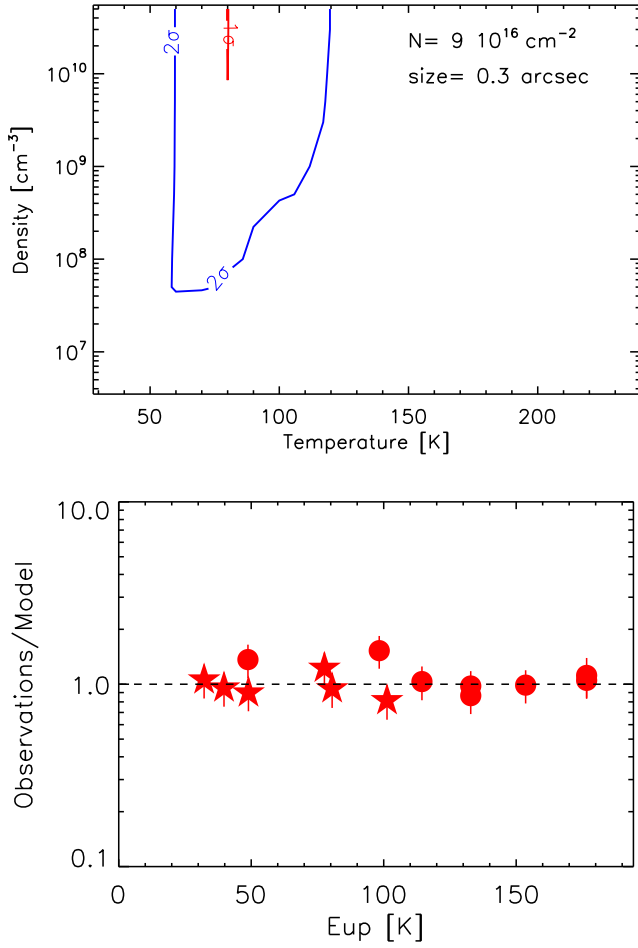


Figure 5. *Upper panel:* The 1σ (in red) and 2σ (in blue) contour plot of χ^2 obtained considering the non-LTE model predicted and observed intensities of the detected $^{13}\text{CH}_3\text{CO}$ lines with $E_{up} > 40$ K. The best fit is obtained with $N(^{13}\text{CH}_3\text{CO}) = 9 \times 10^{16} \text{ cm}^{-2}$, $\theta_s = 0''.3$, $T_{kin} = 80$ K and $n_{\text{H}_2} \geq 3 \times 10^{10} \text{ cm}^{-3}$. *Lower panel:* Ratio between the observed line intensities with those predicted by the best fit model as a function of line upper level energy E_{up} . Circles refer to $^{13}\text{CH}_3\text{CO}$ A transitions while stars refer to E transitions.

Class 0 sources performed by Parise et al. (2006), using data obtained with the same antenna (IRAM 30-m) and a consistent beam sampling. The value measured towards SVS13-A is close to the average value reported for the Class 0 sources, which is $\text{D}/\text{H} \sim 0.12$.

For the double deuterated formaldehyde we obtained a D/H value of $4 \pm 1 \times 10^{-3}$. If we compare this value with that reported by Parise et al. (2006), we can note that it is definitely lower, by at least one order of magnitude, suggesting that the D/H is indeed lower in the more evolved Class I objects, like SVS13-A, with respect to the Class 0 sources.

The D/H value for the D_2CO with respect to the HDCO , is $\sim 5 \times 10^{-3}$, a value again lower of at least one order of magnitude than those reported by Parise et al. (2006) for the Class 0 sources. This estimate is even more reliable because it is independent from H_2^{13}CO .

Finally, we derived the D/H ratio also for the outflowing gas. In this case, we assumed an extended component with a source size of $10''$, obtaining a value of $4 \pm 6 \times 10^{-3}$ for the HDCO in the

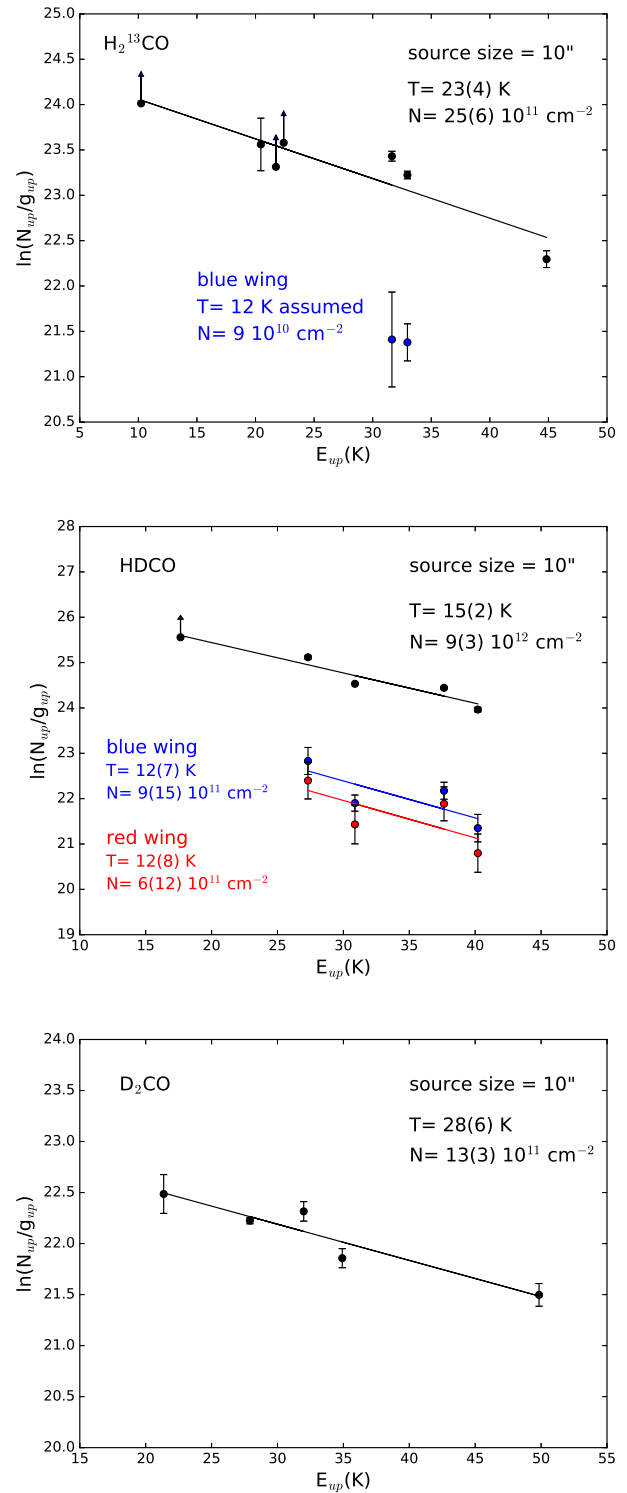


Figure 6. Rotation diagrams for H_2^{13}CO (upper panel), HDCO (middle panel) and D_2CO (lower panel). An emitting region size of $10''$ is assumed (see text). The parameters N_u , g_u , and E_{up} are, respectively, the column density, the degeneracy and the energy (with respect to the ground state of each symmetry) of the upper level. The derived values of the rotational temperature are reported. Arrows are for the lines affected by wobbler contamination (see Section 3.2) and thus considered as lower limits.

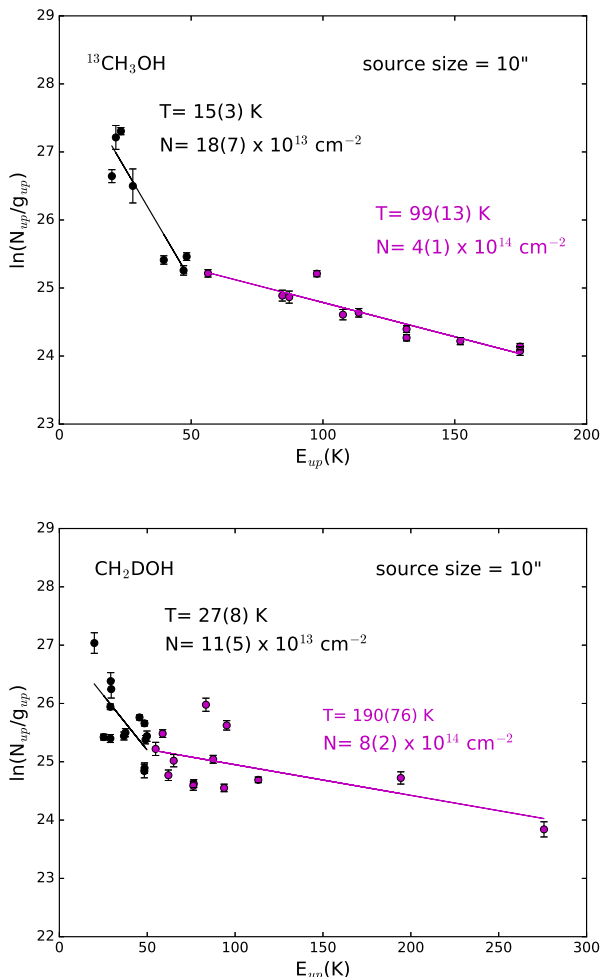


Figure 7. Rotation diagrams for $^{13}\text{CH}_3\text{OH}$ (upper panel) and CH_2DOH (lower panel) assuming two emitting components. An emitting region size of $10''$ is assumed (see text). The parameters N_u , g_u , and E_{up} are, respectively, the column density, the degeneracy and the energy (with respect to the ground state of each symmetry) of the upper level. The derived values of the rotational temperature are reported.

blue wing and $3 \pm 6 \times 10^{-3}$ for the HDCO in the red wing. These measurements are in agreement with that measured in the shocked region associated with the L1157 protostellar outflow by Codella et al. (2012), that reported a value of $5\text{--}8 \times 10^{-3}$ using IRAM 30-m data.

The derived D/H ratio for CH_2DOH with respect to CH_3OH is indicated in Table 3. To calculate this ratio, we derived the CH_2DOH column density assuming the same T_{rot} of $^{13}\text{CH}_3\text{OH}$, obtaining $\text{D}/\text{H} \sim 2 \times 10^{-3}$, for the lines with excitation energies $E_{\text{up}} < 50$ K, and $\text{D}/\text{H} \sim 7 \pm 1 \times 10^{-3}$ for the lines with $E_{\text{up}} > 50$ K. These values are two orders of magnitude below the D/H reported in Parise et al. (2006), supporting that also the methanol deuteration for the Class I object SVS13-A is dramatically decreased with respect to Class 0 objects.

We give an estimate of the CH_2DOH and CH_3OD column densities using the tentative detected two lines, which can be used as lower limits for the following analysis. We derived a value of $N_{\text{tot}} \sim 1 \times 10^{16} \text{ cm}^{-2}$ for CH_2DOH and $N_{\text{tot}} \sim 6 \times 10^{14}$

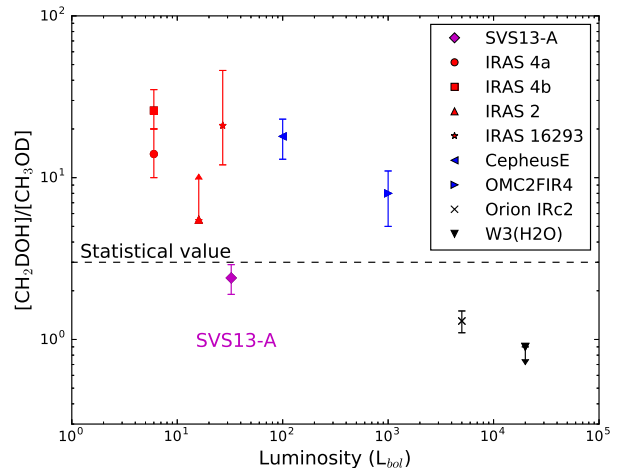


Figure 8. Adapted from Ratajczak et al. (2011). The figure shows the $[\text{CH}_2\text{DOH}]/[\text{CH}_3\text{OD}]$ ratio as a function of the protostar luminosity. The horizontal dashed line refers to the value predicted by grain chemistry models (Charnley et al. 1997).

cm^{-2} for CH_3OD , assuming the same source size and T_{rot} of the $^{13}\text{CH}_3\text{OH}$ low energy transitions (size $\sim 3''$ and $T_{\text{rot}} = 12$ K) and using the rotational partition functions from Ratajczak et al. (2011).

4.4 The $[\text{CH}_2\text{DOH}]/[\text{CH}_3\text{OD}]$ ratio

Finally, we used the detection of CH_3OD to derive a measure of the $[\text{CH}_2\text{DOH}]/[\text{CH}_3\text{OD}]$ ratio, and thus test the predictions of the current theory of methanol deuteration. Basically, according to the grain chemistry statistical models of Charnley et al. (1997) and Osamura et al. (2004) the ratio of the singly deuterated isotopologues CH_2DOH and CH_3OD formed on the mantles should always be 3. However, this is not confirmed by the few measurements in star forming regions.

Figure 9 (from Ratajczak et al. 2011 and reference therein) reports the so far measured ratios as a function of the bolometric luminosity, including both low- and high-mass star forming regions. The $[\text{CH}_2\text{DOH}]/[\text{CH}_3\text{OD}]$ ratio always differs from the statistical value suggesting a weak trend: the abundance ratio is substantially lower in massive hot cores than in (low-mass) hot-corinos (as well as in intermediate-mass protostars), by typically one order of magnitude. In particular, in low mass protostars, CH_3OD is found to be less abundant than CH_2DOH , by more than a factor 10 (Ratajczak et al. 2011). Unless the prediction for the methanol formation on dust grains has to be revised, these measurements are suggesting that the ratio is altered by gas-phase reactions at work once the deuterated methanol molecules are released by the dust mantles.

The present work allows us to provide a little piece of information to this general context. For SVS13-A we obtained $[\text{CH}_2\text{DOH}]/[\text{CH}_3\text{OD}]$ in the 2.0 – 2.5 range (see the magenta point in Figure 9), comparing the column density estimated from the CH_3OD $5_{1+}\text{--}4_{1+}$ line and the column density from a CH_2DOH line with similar energy ($4_{2,3}\text{--}4_{1,4}$ e0). Our measurement seems to question the previous conclusions on a change of the $[\text{CH}_2\text{DOH}]/[\text{CH}_3\text{OD}]$ ratio as a function of the protostellar luminosity. On the other hand, it suggests an evolution with time going from Class 0 to Class I, with CH_2DOH more efficiently destroyed

than CH₃OD. To conclude, it is clear that we need further measurements to properly investigate any possible dependence on time and/or luminosity.

4.5 Deuterium fractionation of organics: from Class 0 to Class I

The present results strongly support that both H₂CO and CH₃OH deuteration decreases when a protostar leaves the Class 0 stage to enter in the Class I phase. Figure 9 shows the D/H ratio measured for organic molecules at different stages of the Sun-like star forming process, from prestellar cores to protoplanetary disks (the time increases from the left to the right along the x-axis). The present observation for SVS13-A can be properly compared with that of Class 0 objects, derived by sampling similar spatial scales around the protostar. The methanol and formaldehyde deuteration measurements of SVS13-A, fill in the gap between Class 0 objects and protoplanetary disks, associated with Class II-III objects.

For HDCO, the average value measured in Class 0 sources (Parise et al. 2006) is D/H \sim 0.12, consistent with the value measured in SVS13-A, which is D/H \sim $8.6 \pm 3.5 \times 10^{-2}$. Completely different is the case of D₂CO, which shows an increase going from prestellar cores (average value D/H \sim 0.045, Bacmann et al. 2003) to Class 0 sources (D/H \sim 0.15, Parise et al. 2006) and then a strong decrease in SVS13-A (D/H = $3.8 \pm 1.1 \times 10^{-3}$). A similar behaviour is observed for the methanol deuteration that increase from a value of D/H \sim 0.1 in prestellar cores (Bizzocchi et al. 2014) to D/H \sim 0.52 in Class 0 (Parise et al. 2006) and then significantly decrease in SVS13-A to D/H = $(1.5 - 7.1) \times 10^{-3}$.

In conclusion, the overall comparison shows a clear trend going from the prestellar cores to the Class 0 objects and to the Class I source. The deuterium fractionation of organics increase going from prestellar cores to Class 0 sources and then decreases up to two orders of magnitude going from Class 0 protostars to the more evolved phases. In protoplanetary disks the few available organics measurements refer to DCN/HCN (Oberg et al. 2012) and DCO⁺/HCO⁺ (van Dishoeck et al 2006, Guilloteau et al. 2006) and are in agreement with the decreasing trend with values between 0.035 and 0.004. Note that the prestellar cores and the Class 0 protostars are not ordered in age thus any trend within the classes is not significant (as in Ceccarelli et al. 2014).

Why does D/H decrease from Class 0 to Class I protostars? Formaldehyde and methanol observed around embedded protostars have been mostly formed at the surface of interstellar grains and have been then evaporated thermally when the temperature exceeds their temperature of sublimation. Two possibilities can therefore be suggested. The decrease of D/H from Class 0 to Class I could be due to (1) warm gas phase chemistry after the evaporation of formaldehyde or methanol; (2) a lower deuteration of icy formaldehyde and methanol in Class I than in Class 0.

Case 1: Warm gas phase chemistry can decrease the deuterium fractionation of formaldehyde and methanol through ion-neutral reactions. Charnley et al. (1997) showed that the CH₂DOH/CH₃OH decreases dramatically by two orders of magnitude at times longer than 3×10^5 yr, because of electronic recombinations that destroy more efficiently CH₂DOH than CH₃OH. The timescale of 3×10^5 yr is consistent with the typical lifetime of Class I protostars (0.2-0.5 Myr; Evans et al. 2009). However, there are two problems with this picture: (i) revised models by Osamura et al. (2004) suggests longer timescales (up to 10^6 yr), and (ii) the dynamical timescale of the material in the hot corino envelope inside the centrifugal radius could be lower (1×10^4 - 1×10^5 yr; Visser et al. 2009). In

addition, the decrease of methanol deuteration occurs when most of the methanol is already destroyed with abundances lower than 1×10^{-8} . Although formaldehyde spends more time in the warm gas due its lower binding energy, it does not show any significant decrease of its deuteration (Charnley et al. 1997, Roberts & Millar 2007).

Case 2: A second possibility is that the decrease of deuteration is due to the gradual collapse of the external shells of the protostellar envelope. The deuterium chemistry is very sensitive to physical (density, temperature) and chemical (CO abundance, H₂ ortho/para ratio) parameters (see Flower et al. 2006). Icy formaldehyde and methanol deuterations increase with the density and with the decreasing temperature during the formation of prestellar cores (see Taquet et al. 2012b, 2013). Taquet et al. (2014) therefore showed that the deuteration of formaldehyde and methanol ices can decrease by two orders of magnitude from the centre to the external part of prestellar cores, the exact values depending on the structure of the core and its history. In the subsequent protostellar phase, the shells are then gradually accreted from the center to the outer part in an inside-out fashion during the core collapse. The methanol deuteration observed in the early Class 0 phase would reflect the material at the center of the prestellar core whereas the older Class I phase reflects the material coming from the external core shells. An instructive view has been reported by Codella et al. (2012), who analysed the H₂CO and CH₃OH deuteration in the shocked region L1157-B1, located relatively far (0.08 pc) from the protostar driving the shocks in the outflow, and thus sampling an outer region probably associated with a (pre-stellar) density lower than that where the protostar is successively born. The D/H derived for L1157-B1 are indeed lower than what found for the standard hot corino IRAS16293-2422, i.e. the inner 100 AU of the protostellar core. In other words, H₂CO and CH₃OH deuteration can be used to measure the density at the moment of the ices formation, before the start of the star forming process: the higher the D/H, the higher the density. In the case of SVS13-A the D/H for formaldehyde in the outflow, sampling a region definitely more extended than the protostellar high density cocoon, is indeed supporting this scenario (see Figure 10). The decrease by two orders of magnitude from Class 0 to Class I protostars observed for the D₂CO/H₂CO and CH₂DOH/CH₃OH ratios is in good agreement with the model predictions by Taquet et al. (2014) within an order of magnitude although the models still tend to underpredict the absolute ratios. It should be noted that the decrease of formaldehyde and methanol deuterations with the evolutionary stage of the protostar are not necessarily accompanied by a decrease of water deuteration. As water ice is mostly formed in molecular clouds before the formation of prestellar cores, its deuteration only weakly varies within prestellar cores. This scenario can therefore simultaneously explain the decrease of deuteration of formaldehyde and methanol observed in this work and, in addition, the constant deuteration of water observed towards SVS13-A by Codella et al. (2016).

5 CONCLUSIONS

We studied the formaldehyde and methanol deuteration in the Class I object SVS13-A with the IRAM 30-m antenna in the framework of the ASAI large program consisting of an unbiased spectral survey at 1.3, 2 and 3 mm towards the source. The aim of this project was to understand how the deuterium fractionation of organics like H₂CO and CH₃OH change in a Class I object, SVS13-A, with respect to the Class 0 sources. The bulk of the detected lines are in

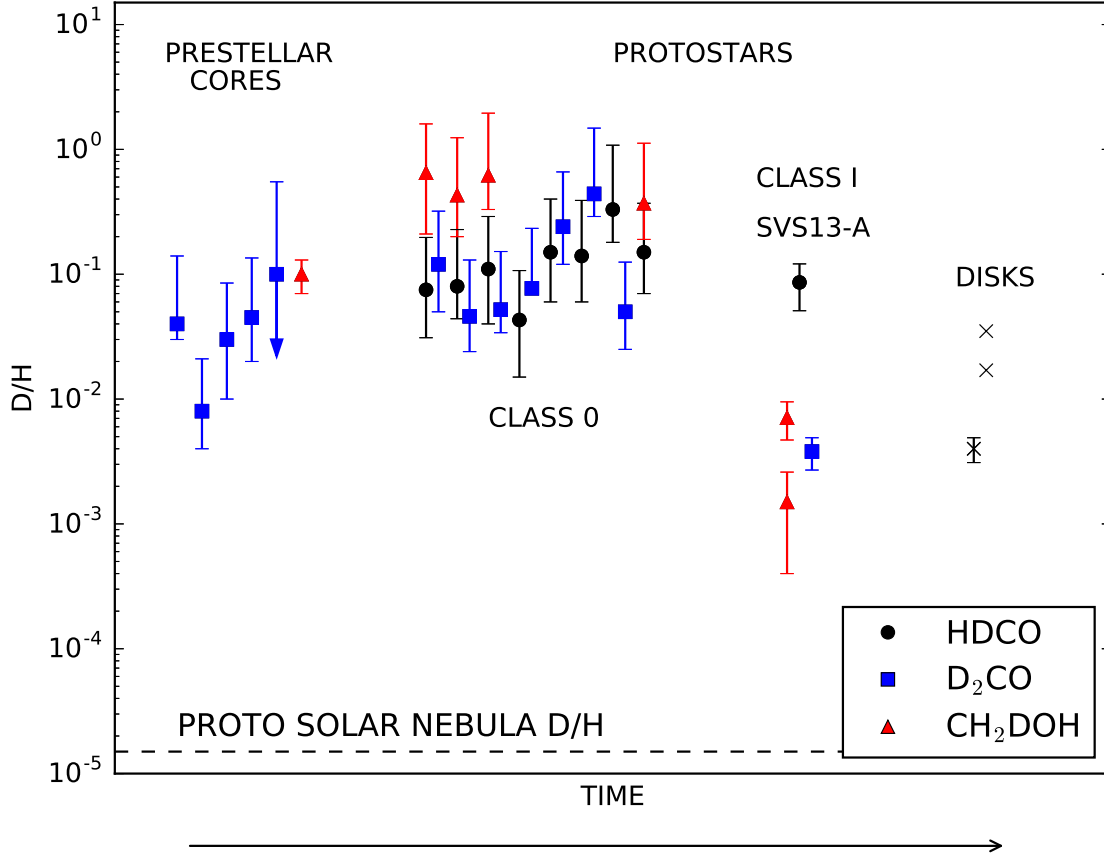


Figure 9. D/H ratio measured in organic matter in different astronomical sources. Prestellar cores measurements of D_2CO and CH_2DOH are from respectively Bacmann et al. (2003) and Bizzocchi et al. (2014). Class 0 data are taken from Parise et al. (2006). SVS13-A data refer to the D/H inferred in the present paper for HDCO (8.6×10^{-2}), D_2CO (3.8×10^{-3}) and CH_2DOH (7.1×10^{-3} for the hot corino and 1.5×10^{-3} for a larger region, i.e. a radius ≤ 350 AU). Protoplanetary disks data refer to measurements of DCN/HCN (Oberg et al. 2012) and DCO^+/HCO^+ (van Dishoeck et al. 2006) in TW Hya and of DCO^+/HCO^+ (Guilloteau et al. 2006) in DM Tau. Note that the prestellar cores and the Class 0 protostars are not ordered in age thus any trend within the classes is not significant (as in Ceccarelli et al. 2014).

the 1.3 mm band corresponding to a telescope HPBW $\sim 10''$. This ensures that the signal is coming from SVS13-A and it is not contaminated by the SVS13-B Class 0 object, offset by $15''$. The main results are reported as follows:

(i) We detected 7 lines of $H_2^{13}CO$, 5 transitions of HDCO and 5 lines of D_2CO with excitation energies E_{up} in the 10-45 K range. The LVG analysis of $H_2^{13}CO$ indicates low values of T_{kin} (~ 20 K), densities larger than 10^6 cm^{-3} , and an emitting size of about $5''$ (~ 1200 AU). The low temperature is confirmed by the rotational diagram performed for all formaldehyde isotopologues, suggesting the association with the molecular envelope surrounding the protostar.

(ii) Both $H_2^{13}CO$ and HDCO lines show wings indicating emission from outflowing gas. For both the blue- and the red-shifted emission we obtained a low T_{rot} (~ 12 K), in agreement with the association with the extended outflow driven by SVS13-A.

(iii) We detected 18 lines of $^{13}CH_3OH$ and 27 transitions of CH_2DOH with E_{up} in the 20-276 K range. We report the detection of CHD_2OH and CH_3OD through 2 different transition for each species. The LVG analysis of $^{13}CH_3OH$ suggests the occurrence of

of two components, with different excitation conditions: (1) a compact region ($\theta_s \simeq 0''.3$, 70 AU) corresponding to high temperatures ($T_{kin} \sim 80$ K) and very high densities ($> 10^8 \text{ cm}^{-3}$), clearly being the hot-corino (recently discovered by HDO observations; Codella et al. 2016). (2) a colder ($T_{kin} \leq 70$ K), more extended ($\theta_s \simeq 2'' - 4''$) region associated with densities $> 10^6 \text{ cm}^{-3}$. The rotation diagram analysis confirms for the deuterated methanol the presence of a hot corino component associated to high densities and temperatures and a second component due to colder gas emission.

(iv) We measured for formaldehyde $D/H \sim 9 \times 10^{-2}$, a value consistent with the average value reported from Class 0 sources ($D/H \sim 0.12$, Parise et al. 2006). The deuterium fractionation derived for the outflowing component is $D/H \sim 4 \times 10^{-3}$, in agreement with those measured in the shocked region associated with the L1157 protostellar outflow by Codella et al. (2012). On the other hand, for D_2CO we obtained $D/H \sim 4 \times 10^{-3}$, lower by one order of magnitude with respect to Class 0 objects. This trend is even stronger for the measured methanol deuteration, which is 4×10^{-3} , two orders of magnitude lower than the values reported by Parise et al. (2006) for Class 0 objects.

Table 3. Results from the rotational diagram analysis: derived rotational temperatures, T_{rot} , derived column densities, N_{tot} , and resulting deuteration ratios. The latter are calculated assuming for each deuterated species, the same T_{rot} of the correspondent 13-isotopologue.

Transition	Lines	Energy range (K)	Boltzmann Plots			D/H^b
			Size ^a (")	T_{rot} (K)	N_{tot} (cm^{-2})	
whole emission						
D ₂ CO	5	21–50	5	25(5)	$3(1) \times 10^{12}$	$3.8(1.1) \times 10^{-3}$
HDCO	5	18–40	5	12(2)	$3(1) \times 10^{13}$	$8.6(3.5) \times 10^{-2}$
H ₂ ¹³ CO	7	10–45	5	19(3)	$7(2) \times 10^{12}$	–
CH ₂ DOH ($E_{\text{up}} < 50$ K)	14	20–50	~ 3	24(9)	$7(5) \times 10^{14}$	$1.5(1.1) \times 10^{-3}$
¹³ CH ₃ OH ($E_{\text{up}} < 50$ K)	7	20–48	~ 3	12(2)	$16(7) \times 10^{14}$	–
CH ₂ DOH ($E_{\text{up}} > 50$ K)	13	54–194	0.3	177(71)	$4(1) \times 10^{17}$	$7.1(2.4) \times 10^{-3}$
¹³ CH ₃ OH ($E_{\text{up}} > 50$ K)	11	56–175	0.3	91(13)	$20(4) \times 10^{16}$	–
outflow						
H ₂ ¹³ CO Blue wing ^c	3	20–33	10	12 ^c	$15(5) \times 10^{11}$	–
HDCO Blue wing ^c	4	27–40	10	12(7)	$9(15) \times 10^{11}$	$4.0(6.3) \times 10^{-3}$
HDCO Red wing ^c	4	27–40	10	12(8)	$6(12) \times 10^{11}$	$2.6(5.2) \times 10^{-3}$

^a Assumed from LVG analysis results; for the outflow component we arbitrarily assumed an extended (10'') size.

^b To calculate the D/H ratio we assumed for HDCO and D₂CO the same rotational temperature of H₂¹³CO ($T_{\text{rot}} = 19$ K). For CH₂DOH we assumed the same rotational temperature of ¹³CH₃OH ($T_{\text{rot}} = 12$ K and 91 K).

^c Derived using the residual intensities after subtracting the gaussian fit of the ambient component. For the H₂¹³CO wings we assumed the same T_{rot} of the HDCO wings (see Text).

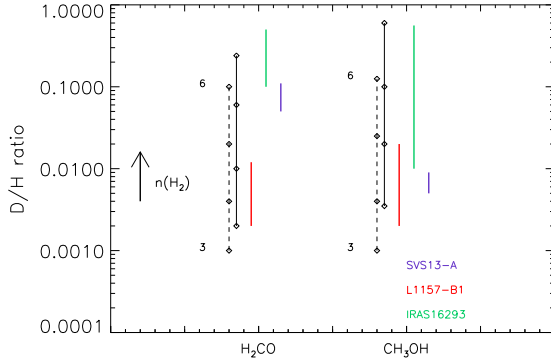


Figure 10. Deuterium fractionation of H₂CO and CH₃OH as found toward SVS13-A (blue), L1157-B1 (red) and IRAS162932422 (green; from Loinard et al. 2001; Parise et al. 2002, 2004). Black diamonds stand for the prediction of Taquet et al. (2012b) for pre-shock gas densities of 10^3 , 10^4 , 10^5 , and 10^6 cm^{-3} (see labels) and temperatures of 10 (dashed line) and 20 K (solid).

(v) The detection of CH₃OD allows us to derive a measure of the [CH₂DOH]/[CH₃OD] ratio that is in the 2.0 - 2.5 range. Previous measurements by Ratajczak et al. (2011), including both low- and high-mass star forming regions, indicate a weak trend with a lower abundance ratio observed in massive hot cores with respect to (low-mass) hot- corinos (as well as in intermediate-mass protostars), by typically one order of magnitude. According to these indications, in SVS13-A CH₃OD was expected to be less abundant than CH₂DOH, by more than a factor 10 (Ratajczak et al. 2011). However our [CH₂DOH]/[CH₃OD] measurement questions the previous indication about a correlation between this ratio and the protostellar luminosity.

(vi) The low deuterium fractionation measured towards SVS13-A could be an indication of the modified chemical content in the evolutionary transition from the Class 0 phase to the Class I phase. Alternatively, the decrease of D/H in a more evolved phase could be due to the gradual collapse of the external shells of the protostellar envelope, less deuterated because composed of ices formed in a less dense region. Only high resolution interferometric observations, able to sample the inner region of the protostar ($< 1''$ corresponding to ~ 235 AU at the source distance) and to disentangle the emission coming from the different protostar components, will properly answer these open questions.

ACKNOWLEDGMENTS

The authors are grateful to the IRAM staff for its help in the calibration of the 30-m data. The research leading to these results has received funding from the European Commission Seventh Framework Programme (FP/2007-2013) under grant agreement N 283393 (RadioNet3). This work was partly supported by the PRIN INAF 2012 – JEDI and by the Italian Ministero dell’Istruzione, Università e Ricerca through the grant Progetti Premiali 2012 – iALMA which is also founding the EB PhD project. BL and CCe acknowledge the financial support from the French Space Agency CNES and RB from Spanish MINECO (through project FIS2012-32096). BL and CCe acknowledge support from the CNRS program Physique et Chimie du Milieu Interstellaire (PCMI) and a grant from LabeX Oug@2020(Investissements d’avenir - ANR10LABX56).

REFERENCES

- Aikawa, Y., Wakelam, V., Hersant, F., et al. 2012, *ApJ*, 760, 40
 Bachiller, R., Guilloteau, S., Gueth, F., et al. 1998, *A&A*, 339, L49
 Bacmann, A., Lefloch, B., Ceccarelli, C. et al. 2003, *ApJ*, 585, L55-L58

- Bizzocchi, L., Caselli, P., Spezzano, S., & Leonardo, E. 2014, *A&A*, 569, A27
- Camargo, D., Bonatto, C., & Bica, E., 2015, *MNRAS*, 450, 4150
- Caselli, P. & Ceccarelli, C., 2012, *A&A Rev.*, 20, 56
- Ceccarelli, C., Caselli, P., Bockelee-Morvan, D. et al. 2014, in *Protostars and Planets VI*, ed. H. Beuther, R. Klessen, C. Dullemond, Th. Henning (University of Arizona Press 2014)
- Ceccarelli, C., Caselli, P., Herbst, E., et al. 2007, in *Protostars and Planets V*, ed. B. Reipurth, D. Jewitt, & K. Keil, 4762
- Ceccarelli, C., Loinard, L., Castets, A., et al. 2001, *A&A*, 372, 998
- Ceccarelli, C., Castets, A., Loinard, L., et al. 1998, *A&A*, 338, L43
- Charnley, S. B., Tielens, A. G. G. M. & Rodgers, S. D. 1997, *ApJL*, 482, L203
- Chen, X., Launhardt, R. & Henning, Th. 2009, *ApJ* 691, 1729
- Chini, R., Reipurth, B., Sievers, A., et al. 1997, *A&A*, 325, 542
- Codella, C., Ceccarelli, C., Bianchi, E., et al. 2016, *MNRAS*, 462, L75
- Codella C., Ceccarelli C., Lefloch B., et al. 2012, *ApJ*, 757, L9
- Codella, C., Bachiller, R. & Reipurth, B. 1999, *A&A*, 343, 585
- Evans, N. J. II., Dunham, M. M., Jrgensen, J. K., et al. 2009, *ApJ*, 181, 321
- Flower, D. R., Pineau Des Forêts, G., & Walmsley, C. M. 2006, *A&A*, 449, 621
- Fontani, F., Codella, C., Lefloch, B., et al. 2014, *ApJL*, 788, L43
- Fuente, A., Neri, R., & Caselli, P. 2005, *A&A*, 444, 481
- Guilloteau, S., Piétu, V., Dutrey, A., & Guélin, M. 2006, *A&A*, 448, L5
- Hirota, T., Bushimata, T., Choi, Y.K., et al. 2008, *PASJ* 60, 37
- Kristensen, L. E., van Dishoeck, E. F., Bergin, E. A. et al. 2012, *A&A*, 542, A8
- Lefloch, B., Castets, A., Cernicharo, J., et al. 1998, *A&A*, 334, 269
- Linsky, J. L. 2007, *Space Sci. Rev.*, 130, 367
- Loinard, L., Castets, A., Ceccarelli, C., et al. 2002, *P&SS*, 50, 1205
- Looney, L. W., Mundy, L. G., & Welch, W. J. 2000, *ApJ*, 529, 477
- López-Sepulcre, A., Jaber, A. A., Mendoza, E., et al. 2015, *MNRAS*, 449, 2438
- Maret, S., Hily-Blant, P., Pety, J., et al. 2011, *A&A* 526, A47
- Milam, S. N., Savage, C., Brewster, M. A., Ziurys, L. M., Wyckoff, S., 2005, *ApJ*, 634, 1126
- Müller, H.S.P., Schlöder, F., Stutzki, J., et al. 2005, *Journal of Molecular Structure*, 742, 215
- Müller, H.S.P., Thorwirth, S., Roth, D.A., et al. 2001, *A&A*, 370, L49
- Öberg, K. I., Qi, C., Wilner, D. J., & Hogerheijde, M. R. 2012, *ApJ*, 749, 162
- Osamura Y., Roberts H., Herbst E., 2004, *A&A*, 421, 1101
- Parise, B., Ceccarelli, C., Tielens, A. G. G. M., et al. 2006, *A&A*, 453, 949
- Parise, B., Castets, A., Herbst, E., et al. 2004, *A&A*, 416, 159
- Parise, B., Ceccarelli, C., Tielens, A. G. G. M., et al. 2002, *A&A*, 393, L49
- Pickett, H.M., Poynter, R.L., Cohen, E.A., et al. 1998, *J. Quant. Spectrosc. & Rad. Transfer* 60, 883
- Ratajczak, A., Taquet, V., Kahane, C., et al. 2011, *A&A*, 528, L13
- Reipurth, B., Chini, R., Krugel, E., Kreysa, E., Sievers, A., 1993, *A&A*, 273, 221
- Roberts, H., & Millar, T. J. 2007, *A&A*, 471, 849
- Roberts, H., & Millar, T. J. 2000b, *A&A*, 364, 780
- Taquet, V., Charnley, S. B., Sipilä, O. 2014, *ApJ* 791, 1
- Taquet, V., Peters, P., Kahane, C., et al. 2013, *A&A*, 550, 127
- Taquet, V., Ceccarelli, C., & Kahane, C. 2012, *ApJ* 784, L3
- Tielens, A. G. G. M. 1983, *A&A*, 119, 177
- Tobin, J. J., Looney, L. W., Li, Z.-Y., et al. 2016, *ApJ*, 818, 73
- van Dishoeck, E. F., Thi, W.-F., & van Zadelhoff, G.-J. 2003, *A&A*, 400, L1
- Vastel C., Ceccarelli C., Lefloch B., et al. 2014, *ApJ*, 795, L2
- Visser, R., van Dishoeck, E. F., Doty, S. D., & Dullemond, C. P. 2009, *A&A*, 495, 881
- Watanabe, Y., Sakai, N., Lindberg, J. E., et al. 2012, *ApJ*, 745, 126